Pergamon

Int. J. Heat Mass Transfer. Vol. 38, No. 17, pp. 3135–3142, 1995

0017–9310/95 $9.50+0.00

0017–9310(95)00084–4

Analysis of laser beam deviation fluctuations in a turbulent nonisothermal flow and relevance to ε_θ

F. EL AMMOURI, A. SOUFIANI and J. TAINE

Laboratoire EM2C, UPR 288 du CNRS et de l'ECP, Ecole Centrale Paris, 92295 Châtenay-Malabry Cedex, France

(*Received* 11 *July* 1994 *and in final form* 14 *February* 1995)

Abstract—The fluctuating displacements of a laser beam crossing a strongly nonisothermal channel air flow have been measured in the range $[10^4$–$3.5\times10^4]$ of the Reynolds number based on the hydraulic diameter. The measured instantaneous displacements are useful data for testing direct numerical simulations of nonisothermal turbulent flows. It is shown that the variances of these displacements are related to two-point correlation functions of temperature and temperature spatial derivatives. A first approach developed here to predict the beam displacement variances is based on a four supplementary equation, near-wall, turbulence model. These variances are shown to be related to components of the dissipation rate ε_θ of temperature fluctuations. A satisfactory agreement between measured and predicted displacement variances is obtained.

1. INTRODUCTION

Measurements of ε_θ, the dissipation rate of temperature variance, are required among other thermal turbulent quantities to qualify both heat transfer modeling and efficiency in the case of turbulent flows. Only a few works deal with these measurements and they are generally based on intrusive methods. Krishnamoorthy and Antonia [1] have measured the three components of ε_θ by using a pair of parallel cold wires in a turbulent boundary layer. A similar work has been carried out by Sreenivasan *et al.* [2], but only in the logarithmic region of the turbulent field. Verollet [3] has deduced the three components of ε_θ from the two-point-temperature-autocorrelation functions in the same region. It is worth noticing that, in these works, the difference between wall and flow temperatures was limited to about 15 K.

On the other hand the three components of ε_θ can be deduced theoretically from direct numerical simulations. However this approach remains limited to low values of the turbulent Reynolds number and the temperature is generally considered as a passive scalar in such simulations [4–7].

In the present study we use the EM2C laboratory wind channel experimental setup described in a previous work [8], in which the mean temperature gradient field has been measured by means of a laser beam deviation method. Only the mean displacements on a position sensor were analyzed in this previous work. The aim of the present paper is to study the fluctuating part of the displacements obtained in the experiments described in ref. [8] and, particularly, their relevance to temperature fluctuations and the dissipation rate ε_θ.

The experimental setup and signal analysis are briefly described in Section 2. More details are given in ref. [8]. The expressions of laser beam displacement variances in terms of temperature and temperature spatial derivative autocorrelation functions are derived in Section 3. In the next section these functions are modeled in terms of the turbulent quantities k, ε, θ and ε_θ, which are calculated from a four supplementary equation turbulence model. Finally, measured and predicted displacement variances are compared in Section 5.

2. EXPERIMENTAL SETUP AND PROCEDURE

2.1. *The EM2C wind channel*

The EM2C wind channel has been described in detail elsewhere [8–11]. Consequently only a brief description is given here. Heated air, at about 393 K, flows inside a horizontal 2 m long wind channel of rectangular cross section (0.03 and 0.15 m in the vertical and transverse directions, respectively). The upper wall is heated electrically and stabilized in our experiments at a temperature T_u of about 530K; the lower one is held to a temperature T_l of about 373K by using a liquid–vapor water phase change. The channel outlet is open to the atmosphere, and the studied flows are then at the atmospheric pressure P_a, which is measured during each experiment.

Two sets of four windows located at 0.5 and 1.7 m from the channel inlet section enable optical measurements at two cross sections of the channel (Fig. 1). The sapphire windows shown in Fig. 1 are 3 mm thick. The laser beam deviation technique described in the

NOMENCLATURE

a	thermal diffusivity
b	attenuation factor
d	laser beam diameter
D	displacement on the photodiode sensor
D_h	hydraulic diameter
k	turbulent kinetic energy
K	Gladstone–Dale constant
L_1	length of the beam trajectory inside the flow
L_2	distance between the plate edge and the position sensor
f	frequency
n	index of refraction
P_a	atmospheric pressure
Pr	Prandtl number
Re	Reynolds number
T	temperature
u	axial velocity
x	axial distance from the inlet of the channel
y	normal distance to the upper horizontal wall
z	direction of the laser beam.

Greek symbols

θ	$\overline{T'^2}/2$
ε	dissipation rate of k
ε_θ	dissipation rate of θ
λ	thermal conductivity
Φ	power spectral density
Λ	integral length scale
λ_θ	Corrsin length scale.

Subscripts

c	related to the recorded signal convolved with a window function
l	related to the lower wall
r	related to the recorded signal
u	related to the upper wall
x	related to the axial distance
y	related to the normal distance.

Superscripts

A'	fluctuating part of A
A^+	dimensionless expression of A
$\bar{A}$	Reynolds average value of A.

following section is simultaneously applied at the two optical sections.

Gas temperature profiles are also measured in the core of the flow by means of two movable type K thermocouples of 0.25 mm diameter equipped with radiation shields, located 3 cm away from the optical sections, and displaced in the flow by micrometric screws. The radiation shields are retracted in the upper wall before proceeding to optical measurements.

2.2. *Experimental procedure and signal analysis*

Measurements are based on laser beam deviations, induced by refractive index variations in the crossed medium, which result from local and instantaneous temperature gradients in an homogeneous medium at constant pressure. Figure 1 shows the optical setup for deviation measurements. In fact, rather than the deviation, the displacement of the laser beam on a position sensor is measured at a distance L_2 from the channel (Fig. 2). Measurements are carried out for different values, y_i, of the distance between the hot wall and the laser beam inlet. The laser sources, position detectors and other experimental equipment are detailed in ref. [8].

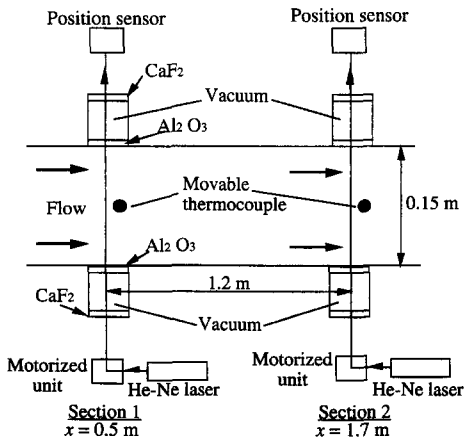

Fig. 1. Schematic view of the studied flow and optical setup.

Temperature fluctuations in turbulent flows induce a time dependence of the laser beam displacement D_i. For each distance y_i, $D_i(t)$ is acquired during a period of time Δt with a sampling frequency f. Δt is chosen long enough (from 0.5 to 3 s) to ensure that $\bar{D}_i$ is time independent (i.e. standard deviation of the time-averaged displacement is less than the experimental noise, which is about 10 μm). The sampling frequency has been chosen in such a manner that the integral of the power spectral density (PSD) of the signal in the range $[0, f/2]$ contains at least 98% of the total power; f varies typically from 2 to 15 kHz in our experimental conditions described in Section 5. For instance, Fig. 3 shows the PSD of the displacement $D_i(t)$ in both x and y directions and for y_i values equal to 1 and 15 mm. In order to estimate the cutoff effect, the extrapolation of the curves for frequencies higher than 7.5 kHz shows that the cutoff at this frequency introduces an error on the total power of about 1%. We ensured that the response of the whole electronic

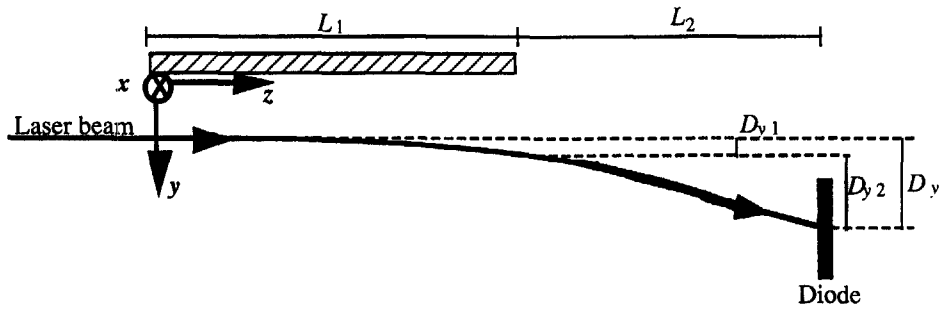

Fig. 2. Scheme of laser beam deviation and displacement (plane perpendicular to the flow direction); definition of axes and geometry ($L_1 = 0.15$ m).

devices remains flat up to the highest sampling frequency.

Another important limitation of displacement measurements at high frequency results from the size of the laser beam whose maximum diameter d inside the flow is about 1 mm. The high frequency components of the signal are attenuated in comparison with those obtained with a ray of null diameter. Indeed, if we adopt a crude one-dimensional model and assume that the beam intensity is uniform in the range $0 \leqslant x \leqslant d$ and that the flow obeys the Taylor hypothesis with an important mean axial velocity $\bar{u}$, the recorded signal $D_r(t)$ is the signal corresponding to a ray $D_c(t)$ convolved with the window function of width $d/\bar{u}$. The attenuation factor $b(f)$ for a given frequency f is then

$$b(f) = \frac{\bar{u}}{\pi f d} \sin\left(\frac{\pi f d}{\bar{u}}\right). \tag{1}$$

In the experimental conditions of Fig. 3, an attenuation factor $b(f) = 0.5$ is reached for $f = 5$ kHz and $f = 7.54$ kHz for $y_i = 1$ mm and $y_i = 15$ mm, respectively. We have estimated the power spectral density $\Phi_c(f)$ of $D_c(t)$ from the spectral density $\Phi_r(f)$ of $D_r(t)$ and $b(f)$:

$$\Phi_c(f) = \frac{\Phi_r(f)}{b^2(f)} \tag{2}$$

and estimated by integration over frequency the total attenuation of the variances $\overline{D_x'^2}$ and $\overline{D_y'^2}$ due to the finite size of the beam. The relative attenuations represent about 5% for $\overline{D_y'^2}$ and about 14% for $\overline{D_x'^2}$. The magnitude of these attenuations is the same for all the experiments described in Section 5.

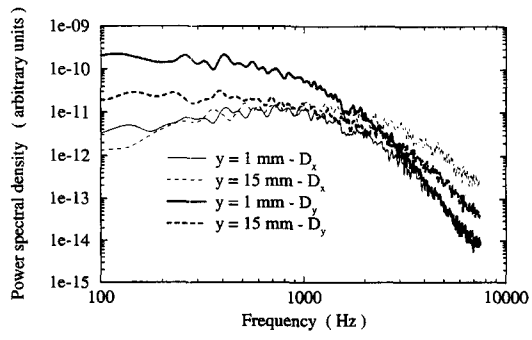

Fig. 3. Power spectral density of the beam displacement at Section 2 vs frequency for experiment E3 [described in Table 1 where $Re_{Dh}(x = 0) = 25\ 200$] and for two different inlet beam positions.

3. EXPRESSIONS OF DISPLACEMENT FLUCTUATIONS AND VARIANCES

A light beam crossing a medium of nonuniform refractive index n is deflected towards the higher n region. For homogeneous gas at constant pressure and for small displacements, the light beam trajectory is described by the following differential equations:

$$\frac{d^2y}{dz^2} = -\frac{K}{T^2}\frac{\partial T}{\partial y}$$

$$\frac{d^2x}{dz^2} = -\frac{K}{T^2}\frac{\partial T}{\partial x} \tag{3}$$

where Oz is the laser propagation direction and K the Gladstone–Dale constant. More details concerning these equations are given in ref. [8]. One can easily show that the beam displacement due to mean temperature gradients inside the sapphire windows are negligible in comparison with those resulting from the temperature gradients in the flow. On the other hand, time scales of heat transfer in the windows are much higher than turbulence characteristic time scales. Consequently, the fluctuating refractive index effects of the windows on the fluctuating part of the displacements can be neglected. The beam displacement on the photodiode sensor can be expressed with the quotations of Fig. 2 as

$$D_y = D_{y1} + D_{y2}. \tag{4}$$

An estimation of the order of magnitude of D_{y1} is obtained from the assumption of a parabolic trajectory of the beam

$$\frac{D_{y1}}{D_{y2}} = \frac{L_1}{2L_2}. \tag{5}$$

This ratio is equal to 0.05 in our experimental conditions. Then neglecting D_{y1} in comparison with D_{y2} leads to

$$D_y \approx D_{y2} = L_2 \frac{\mathrm{d}y}{\mathrm{d}z}(z = L_1). \tag{6}$$

From equations (3) and (6) we obtain

$$D_y = -L_2 \int_0^{L_1} \frac{K}{T^2} \frac{\partial T}{\partial y} \mathrm{d}z. \tag{7}$$

We decompose now T into its mean and fluctuating parts $\bar{T}$ and T' respectively. A second-order Taylor expansion of $1/T^2$ in equation (7) yields

$$D_y = -KL_2 \int_0^{L_1} \frac{1}{\bar{T}^2}\left[\frac{\partial \bar{T}}{\partial y} + \frac{\partial T'}{\partial y} - 2\frac{T'}{\bar{T}}\frac{\partial \bar{T}}{\mathrm{d}y} - \frac{1}{\bar{T}}\frac{\partial \overline{T'^2}}{\partial y} + 3\frac{T'^2}{\bar{T}^2}\frac{\partial \bar{T}}{\partial y}\right]\mathrm{d}z. \tag{8}$$

Time-averaging this equation leads to

$$\bar{D}_y = -KL_2 \int_0^{L_1} \frac{1}{\bar{T}^2}\left[\frac{\partial \bar{T}}{\partial y} - \frac{1}{\bar{T}}\frac{\partial \overline{T'^2}}{\partial y} + 3\frac{\overline{T'^2}}{\bar{T}^2}\frac{\partial \bar{T}}{\partial y}\right]\mathrm{d}z. \tag{9}$$

Then the fluctuating part of the displacement is given by

$$D'_y = D_y - \bar{D}_y = -KL_2 \int_0^{L_1} \frac{1}{\bar{T}^2}\left[\frac{\partial T'}{\partial y} - 2\frac{T'}{\bar{T}}\frac{\partial \bar{T}}{\mathrm{d}y} + 3\frac{(T'^2 - \overline{T'^2})}{\bar{T}^2}\frac{\partial \bar{T}}{\partial y}\right]\mathrm{d}z. \tag{10}$$

If we neglect third order terms, D'^2_y writes

$$D'^2_y = K^2L_2^2 \int_0^{L_1} \frac{1}{\bar{T}^2}\left[\frac{\partial T'}{\partial y} - 2\frac{T'}{\bar{T}}\frac{\partial \bar{T}}{\mathrm{d}y}\right]\mathrm{d}z_1 \times \int_0^{L_1} \frac{1}{\bar{T}^2}\left[\frac{\partial T'}{\partial y} - 2\frac{T'}{\bar{T}}\frac{\partial \bar{T}}{\mathrm{d}y}\right]\mathrm{d}z_2 \tag{11}$$

where z_1 and z_2 are the projections on the z-axis of two independent points of the beam trajectory. Time averaging equation (11) yields

$$\overline{D'^2_y} = K^2L_2^2 \int_0^{L_1}\int_0^{L_1} \frac{1}{\bar{T}^2(z_1)\bar{T}^2(z_2)} \times \left[\overline{\frac{\partial T'}{\partial y}(z_1)\frac{\partial T'}{\partial y}(z_2)} + \frac{4\overline{T'(z_1)T'(z_2)}}{\bar{T}(z_1)\bar{T}(z_2)}\frac{\partial \bar{T}}{\partial y}(z_1)\frac{\partial \bar{T}}{\partial y}(z_2) - \frac{2}{\bar{T}(z_1)}\frac{\partial \bar{T}}{\partial y}(z_1)\overline{T'(z_1)\frac{\partial T'}{\partial y}(z_2)} - \frac{2}{\bar{T}(z_2)}\frac{\partial \bar{T}}{\partial y}(z_2)\overline{T'(z_2)\frac{\partial T'}{\partial y}(z_1)}\right]\mathrm{d}z_1\,\mathrm{d}z_2 \tag{12}$$

which can also be put into the form

$$\overline{D'^2_y} = K^2L_2^2 \int_0^{L_1}\int_0^{L_1} \overline{\frac{\partial}{\partial y}\left(\frac{T'(z_1)}{\bar{T}^2(z_1)}\right)\frac{\partial}{\partial y}\left(\frac{T'(z_2)}{\bar{T}^2(z_2)}\right)}\mathrm{d}z_1\,\mathrm{d}z_2. \tag{13}$$

A similar development may be applied to the laser beam displacement variance in the streamwise direction x. As the mean temperature gradient in this direction is negligible, substituting y for x in equation (13) leads to

$$\overline{D'^2_x} = K^2L_2^2 \int_0^{L_1}\int_0^{L_1} \frac{1}{\bar{T}^2(z_1)\bar{T}^2(z_2)} \times \overline{\frac{\partial T'}{\partial x}(z_1)\frac{\partial T'}{\partial x}(z_2)}\,\mathrm{d}z_1\,\mathrm{d}z_2. \tag{14}$$

We have recorded the instantaneous values of $D'_x(t)$ and $D'_y(t)$ for a set of y_i values. Different statistical informations deduced from these displacements could be compared with direct numerical simulations of the studied flows. In the following, we are mostly interested in the measured variances $\overline{D'^2_x}$ and $\overline{D'^2_y}$, which are compared with the results of a first approach model based on a near-wall turbulence model and dimensional analysis.

4. A FIRST APPROACH MODEL

The laser beam displacement variances given by equations (12) and (14) can be evaluated from the results of a four supplementary equation turbulence model, i.e. the transport equations of the turbulent kinetic energy k, the temperature half-variance $\theta = \overline{T'^2}/2$ and their respective dissipation rates ε and ε_θ. The derivation of the model is given in ref. [15] and the modeled equations, boundary conditions, constants and damping functions may be found in ref. [8].

If we neglect the variations of the mean temperature field along the laser beam, we obtain

$$\overline{D'^2_y} = \frac{K^2L_2^2}{\bar{T}^4}\int_0^{L_1}\int_0^{L_1}\left[\overline{\frac{\partial T'}{\partial y}(z_1)\frac{\partial T'}{\partial y}(z_2)} + \frac{4}{\bar{T}^2}\left(\frac{\partial \bar{T}}{\partial y}\right)^2\overline{T'(z_1)T'(z_2)} - \frac{2}{\bar{T}}\frac{\partial \bar{T}}{\partial y}\frac{\partial(\overline{T'(z_1)T'(z_2)})}{\partial y}\right]\mathrm{d}z_1\,\mathrm{d}z_2 \tag{15}$$

$$\overline{D'^2_x} = \frac{K^2L_2^2}{\bar{T}^4}\int_0^{L_1}\int_0^{L_1}\overline{\frac{\partial T'}{\partial x}(z_1)\frac{\partial T'}{\partial x}(z_2)}\,\mathrm{d}z_1\,\mathrm{d}z_2. \tag{16}$$

The displacement variances depend therefore on the two-point-autocorrelation functions of temperature and temperature spatial derivatives. These autocorrelation functions are modeled as exponentially decaying functions of the separation distance.

$$\overline{\frac{\partial T'}{\partial y}(z_1)\frac{\partial T'}{\partial y}(z_2)} = \overline{\left(\frac{\partial T'}{\partial y}\right)^2}\exp\left[-\frac{|z_2 - z_1|}{\lambda_\theta}\right]$$

$$\overline{T'(z_1)T'(z_2)} = \overline{T'^2}\exp\left[-\frac{|z_2-z_1|}{\Lambda}\right]$$

$$\frac{\partial(\overline{T'(z_1)T'(z_2)})}{\partial y} = \left[\frac{\partial\overline{T'^2}}{\partial y} + \overline{T'^2}\frac{|z_2-z_1|}{\Lambda^2}\frac{\partial\Lambda}{\partial y}\right] \times \exp\left[-\frac{|z_2-z_1|}{\Lambda}\right] \quad (17)$$

where λ_θ and Λ are the Corrsin and the integral length scales of thermal turbulence respectively. λ_θ is modeled using the thermal time scale $\theta/\varepsilon_\theta$ and the thermal molecular diffusivity a [16].

$$\lambda_\theta = c_1\sqrt{a\frac{\theta}{\varepsilon_\theta}} \quad (18)$$

where c_1 is a constant of the model. Numerical simulations show that the best agreement with our experimental data is obtained for $c_1 = 1.4$. The integral length scale Λ is modeled using the turbulent velocity scale $\sqrt{k}$ and a combination of the mechanical time scale k/ε and the thermal time scale $\theta/\varepsilon_\theta$ [17]:

$$\Lambda = c_2\sqrt{k}\sqrt{\frac{k}{\varepsilon}\frac{\theta}{\varepsilon_\theta}} \quad (19)$$

where c_2 is another constant which has a small influence on the results and only in the vicinity of the walls; it is taken equal to 0.5, as in ref. [15].

In our experimental conditions the ratios L_1/Λ and L_1/λ_θ, as calculated from the four equation turbulence model and equations (18), (19), are always greater than 30 and 300, respectively. Consequently, the double integrations in equation (15) with the correlation function (17) become

$$\int_0^{L_1}\int_0^{L_1}\exp\left[-\frac{|z_2-z_1|}{\Lambda}\right]dz_1\,dz_2 = 2\Lambda[L_1-\Lambda]$$

$$\int_0^{L_1}\int_0^{L_1}|z_2-z_1|\exp\left[-\frac{|z_2-z_1|}{\Lambda}\right]dz_1\,dz_2 = 2\Lambda^2[L_1-2\Lambda] \quad (20)$$

and $\overline{D_y'^2}$ is expressed as a sum of three terms:

$$\overline{D_y'^2} = \frac{K^2L_2^2}{\bar{T}^4}\left[A_1\overline{\left(\frac{\partial T'}{\partial y}\right)^2} + A_2 + A_3\right]$$

$$A_1 = 2\lambda_\theta L_1$$

$$A_2 = 16\Lambda\frac{\theta}{\bar{T}^2}\left(\frac{\partial\bar{T}}{\partial y}\right)^2[L_1-\Lambda]$$

$$A_3 = -\frac{8}{\bar{T}}\frac{\partial\bar{T}}{\partial y}\left[\Lambda\frac{\partial\theta}{\partial y}[L_1-\Lambda] + \theta\frac{\partial\Lambda}{\partial y}[L_1-2\Lambda]\right]. \quad (21)$$

In a similar way, if we assume that the same length scale λ_θ applies also for the autocorrelation function in equation (16) we obtain for $\overline{D_x'^2}$

$$\overline{D_x'^2} = \frac{K^2L_2^2}{\bar{T}^4}\overline{\left(\frac{\partial T'}{\partial x}\right)^2}A_1. \quad (22)$$

$\overline{D_x'^2}$ and $\overline{D_y'^2}$ depend then on the terms

$$\overline{\left(\frac{\partial T'}{\partial x}\right)^2} \quad \text{and} \quad \overline{\left(\frac{\partial T'}{\partial y}\right)^2}$$

of ε_θ

$$\varepsilon_\theta = a\left[\overline{\left(\frac{\partial T'}{\partial x}\right)^2} + \overline{\left(\frac{\partial T'}{\partial y}\right)^2} + \overline{\left(\frac{\partial T'}{\partial z}\right)^2}\right]. \quad (23)$$

These quantities cannot be calculated separately from our turbulence model. However, if we make the further assumption

$$\overline{\left(\frac{\partial T'}{\partial z}\right)^2} = \overline{\left(\frac{\partial T'}{\partial x}\right)^2} \quad (24)$$

then

$$\overline{\left(\frac{\partial T'}{\partial x}\right)^2} \quad \text{and} \quad \overline{\left(\frac{\partial T'}{\partial y}\right)^2}$$

can be expressed as functions of ε_θ and the experimental ratio

$$r = \frac{\overline{D_x'^2}}{\overline{D_y'^2}}:$$

$$\overline{\left(\frac{\partial T'}{\partial x}\right)^2} = \frac{r}{(1+2r)A_1}\left[A_1\frac{\varepsilon_\theta}{a} + A_2 + A_3\right]$$

$$\overline{\left(\frac{\partial T'}{\partial y}\right)^2} = \frac{1}{(1+2r)A_1}\left[A_1\frac{\varepsilon_\theta}{a} - 2r(A_2+A_3)\right] \quad (25)$$

and the beam displacement variances are then given in this first approach by

$$\overline{D_x'^2} = \frac{rK^2L_2^2}{(1+2r)\bar{T}^4}\left[A_1\frac{\varepsilon_\theta}{a} + A_2 + A_3\right]$$

$$\overline{D_y'^2} = \frac{K^2L_2^2}{(1+2r)\bar{T}^4}\left[A_1\frac{\varepsilon_\theta}{a} + A_2 + A_3\right]. \quad (26)$$

These variances can be compared to the measured ones. Let notice that in the central flow region ($2 \leqslant y \leqslant 28$ mm), the contributions of A_2 and A_3 in equation (26) are negligible, as shown in Fig. 4, and the ratio r reduces to

$$r = \frac{\overline{D_x'^2}}{\overline{D_y'^2}} = \frac{\overline{\left(\frac{\partial T'}{\partial x}\right)^2}}{\overline{\left(\frac{\partial T'}{\partial y}\right)^2}}. \quad (27)$$

5. RESULTS AND DISCUSSIONS

Experiments have been carried out for five different values of the inlet Reynolds number based on the hydraulic diameter and on the bulk temperature

Table 1. Experimental conditions : $Re_{Dh}(x = 0)$ is the inlet Reynolds number based on the hydraulic diameter, T_u and T_l are, respectively, the temperature of the upper and the lower wall, and P_a is the atmospheric pressure ; $\dot{m}$ is the mass flow rate

Experiment	$Re_{Dh}(x = 0)$	T_u [K]	T_l [K]	P_a ($10^5 \times$ Pa)	$\dot{m}$ (g s^{-1})
E1	10 700	532±15	372±5	$1.016 \pm 1 \times 10^{-3}$	18.4±0.2
E2	17 500	531±15	375±5	$1.017 \pm 1 \times 10^{-3}$	30.0±0.3
E3	25 200	528±15	374±5	$1.004 \pm 1 \times 10^{-3}$	43.1±0.4
E4	30 600	528±15	373±5	$1.007 \pm 1 \times 10^{-3}$	52.3±0.5
E5	35 500	528±15	373±5	$1.007 \pm 1 \times 10^{-3}$	60.7±0.6

$Re_{Dh}(x = 0)$, varying between 10^4 and 3.5×10^4. The experimental conditions, i.e. the Reynolds number, the upper and lower wall temperatures T_u and T_l, the atmospheric pressure P_a and the mass flow rate, are those of ref. [8] and are summarized in Table 1.

Numerical simulations show that the predicted displacement variances at the first measurement section ($x = 0.5$ m) are very sensitive to turbulence intensity at the entrance ($x = 0$), while the predicted displacement variances at the second measurement section ($x = 1.7$ m) do not practically depend on turbulence intensity at the entrance (as shown in the following). As the turbulence intensity at $x = 0$ is not measured in our experiments, only the results related to the second measurement section ($x = 1.7$ m) are presented below. We compare in Figs 5–9 the variances of the laser beam displacements in the x and y directions with the same quantities computed from the first approach model and equations (18), (19), (21), (26). In the last equation, the ratio r is computed from the experimental displacement variances; this fact explains the nonsmoothness of the 'theoretical' curves in Figs 5–9. In the four supplementary equation turbulence model, the inlet turbulence conditions are $k = \varepsilon = \theta = \varepsilon_\theta = 0$, while the mean velocity profile is assumed to be uniform at $x = 0$ (with a value deduced from the measured mass flow rate). The mean temperature profile at section 1 ($x = 0.5$ m) is deduced from the mean laser beam displacements and thermocouple measurements [8].

A satisfactory agreement is found between the model and the experiments in the Reynolds number range mentioned above, especially for y values in the range (2, 28 mm). The agreement is generally better at high Reynolds numbers than at lower ones.

The model overestimates $\overline{D_y'^2}$ near the wall for Reynolds numbers greater than 2.5×10^4. This overestimation results mainly from the assumption that the spanwise and streamwise components of ε_θ are equal [equation (24)]. In fact, as shown in refs. [1, 2], the spanwise component of ε_θ is much greater than the streamwise one in the near wall region. If we introduce the ratio

$$\alpha = \overline{\left(\frac{\partial T'}{\partial z}\right)^2} \Big/ \overline{\left(\frac{\partial T'}{\partial x}\right)^2}$$

in the calculations [equations (20)–(22)], the term $2r$ in the denominator of equation (26) will be replaced by $r(1+\alpha)$. A factor α as high as about 8 is observed in the measurements of ref. [1] for $y^+ \approx 10$. This leads to an overestimation of $\overline{D_y'^2}$, as computed from our

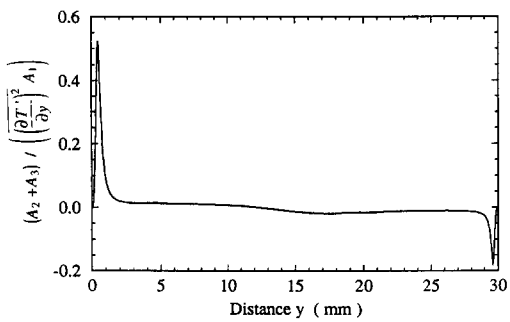

Fig. 4. The ratio $(A_2 + A_3)/(\overline{(\partial T'/\partial y)^2} A_1)$ predicted from the model vs the distance y to the hot wall at Section 2 and for experiment E3 [$Re_{Dh}(x = 0) = 25\,200$].

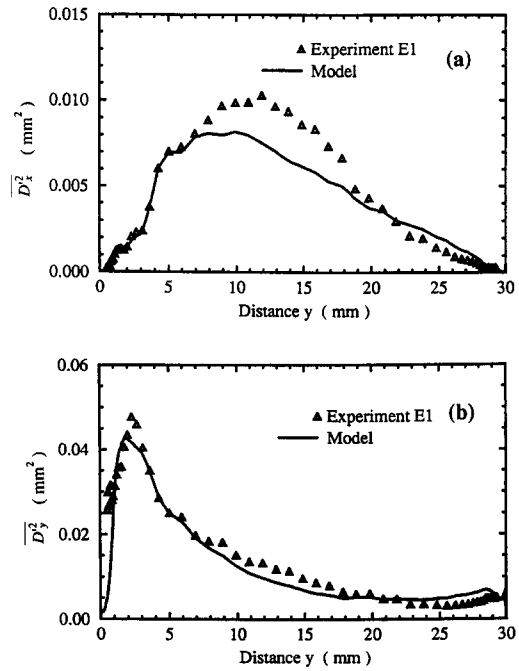

Fig. 5. Measured and predicted displacement variances for experiment E1 [$Re_{Dh}(x = 0) = 10\,700$] at Section 2 vs the distance y to the hot wall. (a) x displacement variance. (b) y displacement variance.

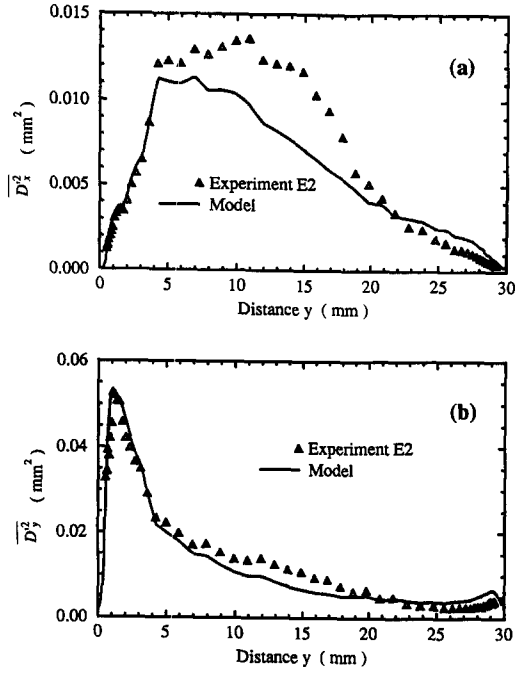

Fig. 6. Same as in Fig. 5 for experiment E2 [$Re_{Dh}(x = 0) = 17\,500$].

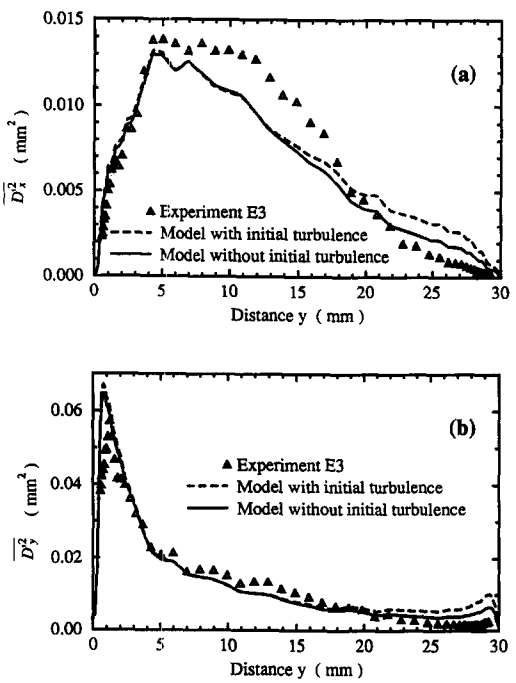

Fig. 7. Same as in Fig. 5 for experiment E3 [$Re_{Dh}(x = 0) = 25\,200$]. The dashed curves correspond to calculation with an initial thermal turbulence intensity equal to 0.15.

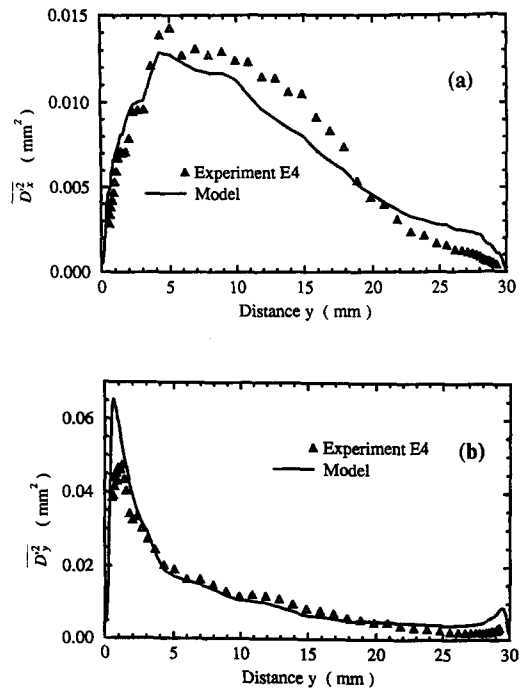

Fig. 8. Same as in Fig. 5 for experiment E4 [$Re_{Dh}(x = 0) = 30\,600$].

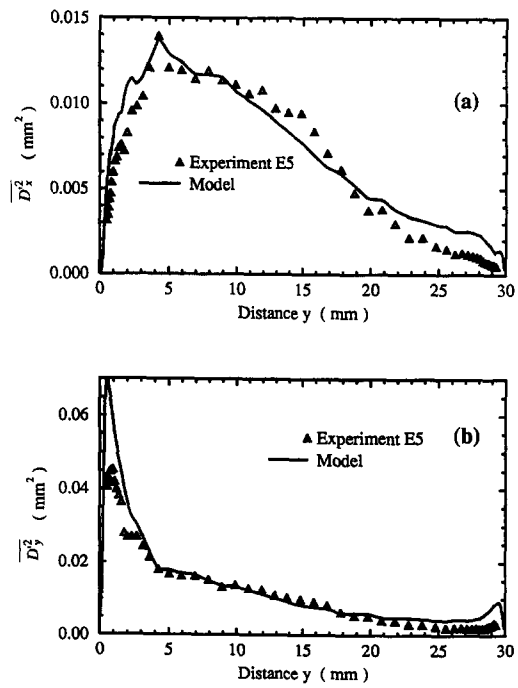

Fig. 9. Same as in Fig. 5 for experiment E5 [$Re_{Dh}(x = 0) = 35\,500$].

first approach model, of about 33%. The discrepancy near the wall is also due, but in a less extent, to the measurement attenuation resulting from the size of the laser beam (see Section 2).

The experimental setup does not allow the measurement of the thermal turbulence intensity $\sqrt{\overline{T'^2}}/\bar{T}$ at the inlet of the channel. The sensitivity of the displacement variances to this initial thermal turbulence has been numerically studied. Figure 7 shows that the variances at Section 2 remain practically unchanged far from the walls, but are significantly increased near the cold wall when considering an initial thermal tur-

bulence intensity of 0.15, which is a large overestimation of the value reached in our experimental conditions.

6. CONCLUDING REMARKS

The fluctuating displacements of a laser beam crossing a strongly nonisothermal channel air flow have been measured in the range (10^4–3.5×10^4) of the Reynolds number, based on the hydraulic diameter. The variances of these displacements have been shown to be related to two-point correlation functions of temperature and temperature spatial derivatives. The experimental data obtained in this study are useful for testing direct numerical simulations of nonisothermal turbulent channel flows. As a first approach, a four supplementary equation, near-wall turbulence model has been used to predict the beam displacement variances which are related to two components of the dissipation rate ε_θ of temperature fluctuations. A satisfactory agreement between measured and predicted displacement variances is found. The agreement is generally better at high Reynolds numbers than at lower ones. The discrepancies observed near the walls is probably due to the anisotropy of ε_θ, which is not fully accounted for in our simulations.

Acknowledgement—The authors are grateful to CNRS—Ecotech for financial support.

REFERENCES

1. L. V. Krishnamoorthy and R. A. Antonia, Temperature dissipation measurements in a turbulent boundary layer, *J. Fluid Mech.* **176,** 265–281 (1987).
2. K. R. Sreenivasan, R. A. Antonia and H. Q. Danh, Temperature dissipation fluctuations in a turbulent boundary layer, *Phys. Fluids* **20,** 1238–1249 (1977).
3. E. Verollet, Etude d'une couche limite turbulente avec aspiration et chauffage à la paroi, Thesis, Université d'Aix-Marseille II (1972).
4. J. Kim, Investigation of heat and momentum transport in turbulent flows via numerical simulations. In *Transport Phenomena in Turbulent Flows* (Edited by M. Hirata and N. Kasagi), pp. 715–730. Hemisphere, New York (1988).
5. J. Kim and P. Moin, Transport of passive scalars in a turbulent channel flow. In *Turbulent Shear Flows*, Vol. 6, pp. 85–96. Springer, Berlin (1989).
6. S. L. Lyons, T. M. Hanratty and J. B. McLaughlin, Direct numerical simulation of passive heat transfer in a turbulent channel flow, *Int. J. Heat Mass Transfer* **34,** 1149–1161 (1991).
7. N. Kasagi, Y. Tomita and A. Kuroda, Direct numerical simulation of the passive scalar field in a two-dimensional channel flow, *ASME/JSME Thermal Engineering Proc.*, Vol. 3, pp. 175–182, Reno (1991).
8. F. El Ammouri and J. Taine, Measurement of wall conductive heat flux in turbulent gas flow by laser beam deflection, *Int. J. Heat Mass Transfer* **37,** 1759–1771 (1994).
9. A. Soufiani and J. Taine, Experimental and theoretical studies of combined radiative and convective transfer in CO_2 and H_2O laminar flows, *Int. J. Heat Mass Transfer* **32,** 477–486 (1989).
10. A. Soufiani and J. Taine, High-resolution spectroscopy temperature measurements in laminar channel flows, *Appl. Opt.* **27,** 3754–3760 (1988).
11. A. Soufiani, Etudes théoriques et expérimentales des transferts couplés par convection laminaire ou turbulente et rayonnement dans un milieu gazeux à température élevée, Thèse d'Etat, Université Paris XI, Orsay (1987).
12. J. O. Hinze, *Turbulence : an Introduction to its Mechanism and Theory*, pp. 174–190. McGraw-Hill, New York (1959).
13. W. P. Jones, B. E. Launder and I. Dekeyser, The prediction of laminarization with a two-equation model of turbulence, *Int. J. Heat Mass Transfer* **15,** 301–314 (1972).
14. C. K. G. Lam and K. A. Bremhorst, A modified form of the k-ε model for predicting wall turbulence, *J. Fluids Engng* **103,** 456–460 (1981).
15. P. Mignon, Etude théorique du couplage convection turbulente-rayonnement dans un écoulement de gaz dans un canal. Thermodégradation de la paroi, Thesis, Ecole Centrale Paris (1992).
16. H. Tennekes and J. L. Lumley, *A First Course in Turbulence*, pp. 95–96. MIT Press, Cambridge, MA (1972).
17. Y. Nagano and C. Kim, A two-equation model for heat transport in wall turbulent shear flows, *J. Heat Transfer* **110,** 583–589 (1988).